Design of Ice Protection Systems and Icing Certification Through the FENSAP-ICE System

Wagdi G. Habashi, Pascal Tran, Guido Baruzzi
Martin Aubéand Pascal Benquet
Newmerical Technologies International
680 Sherbrooke Street West, 7th Floor
Montreal, QC, Canada, H3A 2M7

Summary

The process of certifying a component or system for operation in an icing environment involves two basic steps, analysis and design, followed by icing tests, both of which can be streamlined by the use of 3-D CFD icing technology. The FENSAP-ICE modular system was conceived to support both design and certification of ice protection systems. The droplet impingement module is used to accurately predict high catch regions, which may require protection. These predictions can be obtained for complex 3-D geometries such as swept wings, air induction systems, radomes and complete aircraft or rotorcraft. The ice accretion module is used to compute ice shapes on unprotected surfaces. The heat load module is used to optimize power output required to protect critical surfaces.

Thus, the judicious use of 3-D CFD technology in the design methodology of ice protection systems yields high-performance configurations for operation in icing conditions and thus reduces or focuses the scope of development testing. In addition, CFD can be used in the certification process to pinpoint the most critical conditions in order to produce a smaller test matrix, but yet ensure adequate coverage of the flight and icing envelopes. The present paper shows validation results of FENSAP-ICE and illustrates examples of the application of 3-D CFD icing technology in support of icing certification.

Introduction

Aircraft icing regulations in the United States have evolved greatly over the years. The federal government started regulating pilots and aircraft in 1928 by the creation of the Civil Aviation Agency, which published the Civil Air Regulations or CARs. Prior to 1945, airplanes were certified to CAR 4. The sole reference to aircraft icing in CAR 4 was in Section 04.5814, which required that if deicer boots were installed, then positive means must be provided for the deflation of all wing boots. In 1945, the CARs were divided into two broad categories: CAR 3 for general aviation airplanes, or Part 23 in the modern Code of Federal Regulations (CFR), and CAR 4 for transport airplanes, or Part 25 in the modern CFR. The requirement of Section 04.5814 was incorporated without change as §3.541, which later was renumbered §3.712 in 1949. In 1953, Section 04.5814 became CAR §4.640 and was modified to include the requirement that for pneumatic deicers, two independent power sources shall be provided. Icing envelopes similar to the current Part 25 Appendix C were introduced in CAR 4 in 1955. There were two significant differences between the icing envelope introduced at that time and the current one: the minimum mean effective droplet diameter for intermittent maximum conditions was 20 microns as compared to the current 15 microns and the LWC/distance factor was 1.5 statute miles versus the current 0.26 nautical miles. The icing envelope was revised in 1957 to the current Appendix C. Ice protection was not addressed in CAR 3 until 1962. During that year, Amendment 3-7 added two articles §3.772 and §3.778, which required that the information provided to the crew specifies the types of operation and the meteorological conditions to which the airplane was limited by the equipment installed. In 1964, CAR 3 became Part 23 when §3.712 was recodified to become §23.1419. §3.772 and §3.778(h) became §23.1559

Paper presented at the RTO AVT Symposium on "Reduction of Military Vehicle Acquisition Time and Cost through Advanced Modelling and Virtual Simulation", held in Paris, France, 22-25 April 2002, and published in RTO-MP-089.

and §23.1583(h), respectively. In 1965, CAR 4 was recodified and §4.640 became §25.1419. Since that time the icing regulations have been modified through successive amendments to address propeller, pneumatic deicers, engine installation and several other issues affecting performance of the airplane in icing conditions.[1,2,3]

Currently, demonstration of aircraft compliance to the icing certification requirements is a complex process, which may involve design, analysis and test of several components or systems such as propellers, engines, air induction system, airframe, ice detectors, probes and ice protection systems. The choice of the means of compliance is made through the establishment of a compliance plan, which can include testing, analysis and similarity as means of demonstrating compliance of all systems.

It is believed that design, analysis and testing of an aircraft or rotorcraft for flight in icing conditions can be streamlined by the use of 3-D CFD icing technology. The FENSAP-ICE system originated from an idea enunciated in Ref.[4] took form in successive modules (flow, impingement, accretion, heat loads, performance degradation) described in Refs.[5-9] The FENSAP-ICE system was conceived to support both design and certification of ice protection systems. The droplet impingement module is used to accurately predict high catch regions, which may require protection. These predictions can be obtained for complex 3-D geometries such as swept wings, air induction systems, radomes and complete aircraft or rotorcraft. This type of analysis is sufficient to determine adequate coverage for pneumatic boots or optimal geometry for inertial separation systems. However, for hot air deicing or anti-icing systems, the external wet air calculation is coupled interactively with the internal flow problem and conduction through the solid interface, thereby necessitating a conjugate heat transfer approach. This procedure allows the calculation of minimum anti-icing heat loads required to prevent hazardous ice accretion and water runback. Thus, the judicious use of 3-D CFD technology in the design methodology of ice protection systems yields high-performance configurations for operation in icing conditions and therefore reduces or focuses the scope of development testing. In addition, CFD can be used in the certification process to pinpoint the most critical conditions in order to produce a smaller test matrix, but yet ensure adequate coverage of the flight and icing envelopes. As not all certification conditions can be tunnel-tested, flight-tested, nor encountered in natural icing testing, only analytical methods can make it possible to safely explore, even if only qualitatively, the entire icing envelope.

Advanced notions of using CFD for coupled aerodynamics and icing, using CFD to assess the stability and control of iced aircraft or building a CFD-based in-flight icing simulator, currently absent from the icing community, are within our reach. These state-of-the-art applications of icing CFD technology will ensure vastly improved pilot training and increase our understanding of aircraft flight characteristics in icing conditions, thereby resulting in an increase in flight safety in adverse environmental conditions.

Thus, we advocate that a 3-D Navier-Stokes system is the concurrent engineering tool needed between aerodynamics and icing groups to exchange pre-design information that enhances safety without compromising performance. This is made possible because the icing analytical tools are slowly catching up with the level of sophistication of aerodynamic analyses used to design the aircraft, e.g. 3-D CFD, CAD-based, advanced visualization, multi-disciplinary couplings, inverse design and optimization. Icing can be considered much earlier in the design stages because the incremental cost of the impingement calculation and ice growth prediction is very small compared to the investment required to generate a CAD-based mesh and to solve for the flow at different conditions. Even though 3-D CFD computations may seem intimidating in terms of complexity and CPU time, their cost pales in comparison to a test flight or, worse, an incident or an accident. In addition, any well-written 3-D system like FENSAP-ICE, can be degraded to a 2-D mode, to steady flow, to inviscid flow; simplifications often used in early design stages.

Description of FENSAP-ICE

As shown in Figure 32, FENSAP-ICE is a suite of modules designed for the performance prediction of a system or component in an icing environment. The modularity of FENSAP-ICE is reflected by the fact that each calculation module could be replaced by a commercial package or proprietary code with equivalent functionality.

- FENSAP[5], the Euler/Navier-Stokes solver, can be interchanged with an existing flow solver, which would be coupled to FENSAP-ICE through software interfaces. FENSAP is used for the initial aerodynamic calculation, as well as for the prediction of performance degradation due to the presence of ice[6]. The k-epsilon and k-omega two-equation models are available both as low-Reynolds and high-Reynolds versions. In addition, the Spalart-Allmaras one-equation model is also implemented, with surface roughness and transition.

- DROP3D[7] is an Eulerian particle-tracking module used to compute the catch efficiency distribution on 3-D complex bodies. DROP3D can be used to simulate supercooled water droplets or snow particles. Both FENSAP and DROP3D use a weak-Galerkin finite element method.

- ICE3D[8] is a 3-D ice growth calculation module, or 2.5-D following the surface, and is based on the finite volume method. Surfaces altered by ice accretion are hugged automatically by an Arbitrary Lagrangian-Eulerian (ALE) moving grid method inside the flow solver.

- CHT3D[10] is a conjugate heat transfer interface to couple the convection heat transfer calculations with the conduction through the solid medium. It is crucial for hot air ice protection systems design and analysis.

- Finally, OptiMesh[11] is an anisotropic automatic mesh adaptation module. Starting from a rapidly generated grid, OptiMesh will move grid points, refine edges, coarsen edges and swap edges, to yield a nearly-optimal mesh for the geometry and flow conditions at hand and greatly increase accuracy, besides drastically reducing mesh generation efforts.

All the modules are interlinked seamlessly so as to render possible complex multi-physics calculations such as hot air ice protection with wet air, droplet impingement and runback as illustrated in Ref.[10] Figure 32 illustrates the interaction between all modules.

The last component of the FENSAP-ICE suite is the graphical user interface (GUI), which cements all modules seamlessly. The FENSAP-ICE GUI is quite advanced and comprises file management, window-based inputs, convergence and global values dynamic monitoring, job launch on networks, multi-domain and multi-solver calculations and results archiving. The ease-of-use and complete integration of the icing analysis process reduces engineering time, and therefore costs, ensures traceability and repeatability, and eliminates errors of data transfer between disjoint codes. Figure 33 shows some screen shots of the FENSAP-ICE GUI.

Validation

FENSAP-ICE's flow, impingement, accretion, heat loads and degradation models have been extensively validated against experimental data.[5-8,12,13] FENSAP-ICE's impingement module DROP3D is further validated in the present paper against experimental impingement data gathered by NASA on a 3-D non-axisymmetric Boeing 737 nacelle inlet.[14]

An Euler analysis flow solution was obtained on a tetrahedral mesh. Two cases were analyzed at different incidences of the nacelle, at a true airspeed of 173.33 mph, inlet mass flow of 22.96 lbm/s, droplet Mean Volumetric Diameter of 20.36 μm, and nacelle incidences of 0 (run id 092385-1,2,3-737-0 in Ref.[14]) and

15 deg. (run id 092385-13,14,15-737-15 in Ref.[14]). The comparison of Mach number distributions along circumferential cuts for both incidences is presented in Figures 1 to 10. In order to compute the local catch efficiency β, DROP3D was run for a Langmuir-D droplet distribution. The comparisons of local catch efficiency distribution along the same circumferential cuts are presented in Figures 11 to 20.

The calculated Mach number distributions are in very good agreement with experimental data for all circumferential positions at both incidences.

The comparison between DROP3D and experimental data is very good for most circumferential positions for both incidences. The limits of impingement are correctly predicted and the local catch efficiency peak is also within experimental repeatability estimated in Ref.[14] to vary by 0.20 to 0.25.

The curve for 15 deg. incidence and 135 deg. circumferential position is, however, not in close agreement with the experimental data. Nevertheless, the predictions of LEWICE are even further from the experiments. Since the comparison at zero incidence for the same circumferential position is very good and all the other comparisons at 15 deg. incidence are also quite acceptable for both codes, it is only logical to conclude that the difference for that particular curve may be due to experimental inaccuracies.

Figure 21 illustrates the gain in accuracy that can be achieved by using anisotropic mesh adaptation. The original mesh had 108 000 nodes and 624 000 tetrahedra. After two adaptation cycles, the mesh size increased to 152 000 nodes and 824 000 anisotropic tetrahedral elements. The increased smoothness of the mesh and solution becomes readily apparent when comparing the unadapted mesh and solution shown in Figures 22 and 23 to the adapted mesh and Mach number distribution presented by Figures 24 and 25 respectively.

The ice growth module ICE3D has also been validated against 2-D test cases and 3-D geometries such as a sphere and a helicopter blade.[13]

Numerical Results

Some examples of industrial applications are presented. Because of the proprietary nature of the test cases, only a limited number are shown and the results are only discussed in a qualitative fashion.

Figures 26, 27 and 28 show the structured mesh, streamlines and catch efficiency distribution, respectively, calculated on a helicopter upper cowl with a side-facing inlet. The upper cowl, rotor mast, engine compartment and radial engine intake case down to the first rotor were modeled using a multi-block structured hexahedral mesh. The presence of the inlet screen was neglected. The results shown are for forward flight conditions. Since the engine is installed with the cold end towards the rear, the flow follows the upper cowl skin, turns 90 degrees into the engine plenum and finally turns another 90 degrees into the engine radial intake. The flow field was obtained with a proprietary FENSAP-like viscous flow solver. With the DROP3D Eulerian approach to droplet impingement, the trajectories forming the capture tube of the air induction system were obtained as a post-processing step. For complex geometries, this is vastly more efficient than the hit-and-miss Lagrangian approach to calculate capture tube areas and therefore the ingested water flow rates. This type of capture tube analysis can be used in support of certification to demonstrate that, for side-facing helicopter inlets, forward flight conditions in wet air are very mild in comparison with hover. This is due to the very strong inertial separation effect of the side-facing inlet.

Figures 29, 30 and 31 show the unstructured adapted mesh, Mach number distribution and catch efficiency distribution predicted on a helicopter upper cowl with a forward-facing inlet. The results are shown for a forward flight condition. Several droplet sizes and engine mass flows were simulated in order to understand the effect of engine power on water capture due to the scoop effect of the forward-facing inlet. The analysis was required because an engine growth had to be considered while the geometry of the

air induction system would remain unchanged. In order to determine the necessity of repeating the air induction system icing certification, the potential water ingestion increase had to be quantified. First, a map of mass flow increase as a function of altitude and ambient temperature was constructed for different flight phases such as hover, climb, cruise and descent. Using FENSAP-ICE to calculate droplet impingement, this map was translated to a water capture increase map. Superimposing the Appendix C icing envelope on this map highlighted critical conditions. Decision whether to repeat icing tests is based on such an analysis.

These examples demonstrate the efficiency of the Eulerian particle tracking approach for complex three-dimensional configurations. Because collection efficiency is obtained on all walls and water volume fraction is obtained everywhere in the field, the method yields the particle trajectories of interest as a post-processing step.

Conclusions

FENSAP-ICE, a complete in-flight icing CFD simulation package, was developed to tackle industrial problems involving complex three-dimensional bodies in a timely and cost-effective way. Its accuracy for droplet impingement prediction was demonstrated on a non-axisymmetric nacelle geometry. It can help reduce the amount of testing required by demonstrating the severity, or lack thereof, of certain certification conditions in an accurate, scientific, repeatable and traceable manner. The use of icing CFD in support of aircraft certification offers enormous advantages such as the elimination of the need for scaling or similitude studies, the exploration of the complete icing envelope in a risk-free fashion, the synergy between methods used to design the aircraft and ice protection systems, the elimination of experimental inaccuracies generally associated with icing tests (measurement and control of droplet size, relative humidity, ambient temperature, water flow rate), all of which lead to significant cost reduction.

Although certain phenomena or interaction cannot be simulated at this moment, it is believed that advanced CFD technology, used hand in hand with tunnel or flight tests, can considerably shorten the certification cycle time, reduce the associated costs, reduce post-certification issues and more importantly, increase flight safety in adverse atmospheric conditions.

Future Work

Additions are planned to further increase the range of problems that can be simulated using FENSAP-ICE: SLD models, ice shedding models, ice particle trajectory tracking, one-shot MVD calculations, droplet splashing and breakup, simulation of electro-thermal heater pads, simulation of sand, dust, hail and rain particles, stability and control of iced aircraft, etc.

To further enhance the ease-of-use and integration aspects of FENSAP-ICE, it is planned to very shortly integrate proprietary data post-processing and visualization to the package.

Acknowledgements

NTI would like to thank its industrial partners for permission to present the certification results included in this paper.

References

[1] Chamberlain, H.D., "How Icing Regulations Came to Be", http://www.faa.gov/avr/afs/news/NovemberDecember/IcingReg.htm, Federal Aviation Administration website.

[2] Federal Aviation Administration, "Certification of Part 23 Airplanes for Flight in Icing Conditions", Advisory Circular AC 23.1419-2A, August 1998.

[3] Federal Aviation Administration, "Certification of Transport Airplanes for Flight in Icing Conditions", Advisory Circular 25.1419-1, August 1999.

[4] Habashi, W.G., "Putting Computers on Ice", *ICAO Journal*, Vol. 50, No. 7, October 1995, pp. 14-17.

[5] Baruzzi, G.S., Habashi, W.G., Guèvremont, G. and Hafez, M.M., "A Second Order Finite Element Method for the Solution of the Transonic Euler and Navier-Stokes Equations", *International Journal of Numerical Methods in Fluids*, Vol. 20, pp. 671-693, 1995.

[6] Dompierre, J., Cronin, D., Bourgault, Y., Baruzzi, G. and Habashi, W.G., "Numerical Simulation of Performance Degradation of Ice Contaminated Airfoils", AIAA Paper 97-2235, 15th AIAA Applied Aerodynamics Conference, Atlanta, June 1997.

[7] Bourgault, Y., Habashi, W.G., Dompierre, J. and Baruzzi, G.S., "A Finite Element Method Study of Eulerian Droplets Impingement Models", *International Journal of Numerical Methods in Fluids*, Vol. 29, pp. 429-449, 1999.

[8] Bourgault, Y., Beaugendre, H. and Habashi, W.G., "Development of a Shallow Water Icing Model in FENSAP-ICE," *AIAA Journal of Aircraft*, Vol. 37, pp. 640-646, 2000.

[9] Croce, G. and Habashi, W.G. "Thermal Analysis of Wing Anti-Icing Devices", in "Computational Analysis of Convection Heat Transfer", G. Comini and B. Sundén (Eds.), Wessex Institute of Technology Press, 2000, Chapter 10, pp. 409 -432.

[10] Croce, G., Beaugendre, H. and Habashi, W.G., "CHT3D: FENSAP-ICE Conjugate Heat Transfer Computations with Droplet Impingement and Runback Effects", AIAA Paper 2002-0386, 40th Aerospace Sciences Meeting & Exhibit, Reno, January 2002.

[11] Habashi, W.G., Dompierre, J., Bourgault, Y., Fortin, M. and Vallet, M.-G., "Certifiable Computational Fluid Dynamics Through Mesh Optimization", Invited Paper in Special Issue on Credible Computational Fluid Dynamics Simulation, *AIAA Journal*, Vol. 36, 1998, No. 5, pp. 703-711.

[12] Morency, F., Beaugendre, H., Baruzzi, G.S. and Habashi, W.G., "FENSAP-ICE: A Comprehensive 3D Simulation Tool for In-flight Icing", AIAA Paper 2001-2566, 15th AIAA Computational Fluid Dynamics Conference, Anaheim, CA, June 2001.

[13] Beaugendre, H., Morency, F. and Habashi, W.G., "ICE3D, FENSAP-ICE's 3D In-Flight Ice Accretion Module", AIAA Paper 2002-7134, 40th Aerospace Sciences Meeting & Exhibit, Reno, January 2002.

[14] Papadakis, M., Elangonan, R., Freund, G.A., Breer Jr., M., Zumwalt, G.W. and Whitmer, L., "An Experimental Method for Measuring Water Droplet Impingement Efficiency on Two- and Three-Dimensional Bodies", NASA CR-4257, DOT/FAA/CT-87/22, November 1989.

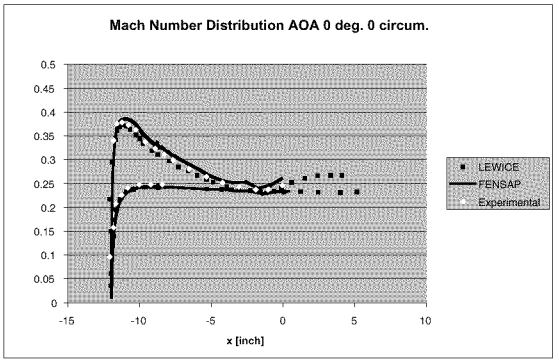

Figure 1: Mach number comparison for zero incidence and 0 deg. circumferential position

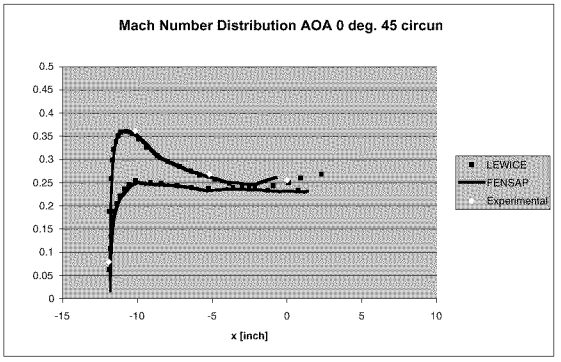

Figure 2: Mach number comparison for zero incidence and 45 deg. circumferential position

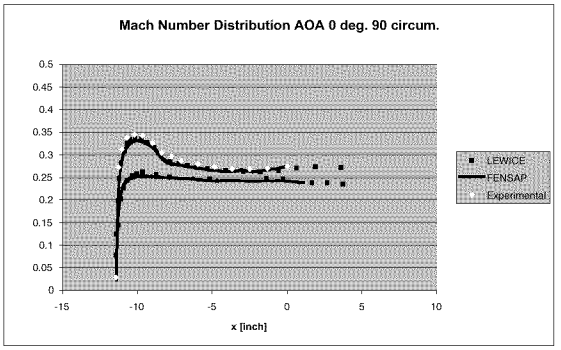

Figure 3: Mach number comparison for zero incidence and 90 deg. circumferential position

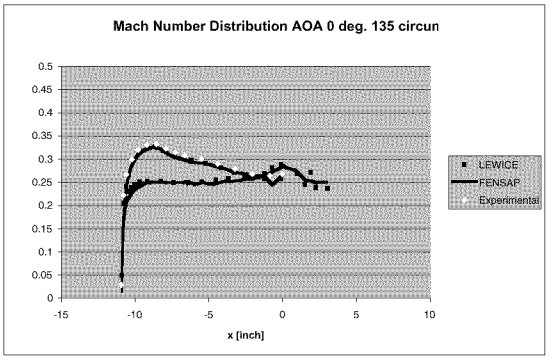

Figure 4: Mach number comparison for zero incidence and 135 deg. circumferential position

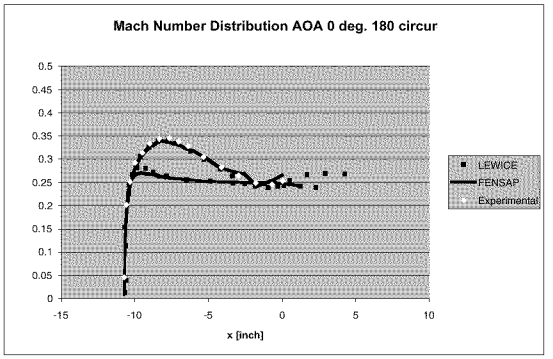

Figure 5: Mach number comparison for zero incidence and 180 deg. circumferential position

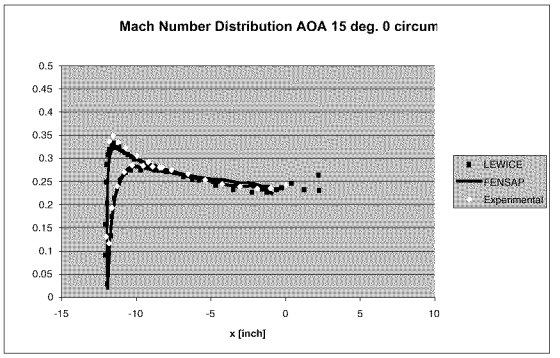

Figure 6: Mach number comparison for 15 deg. incidence and 0 deg. circumferential position

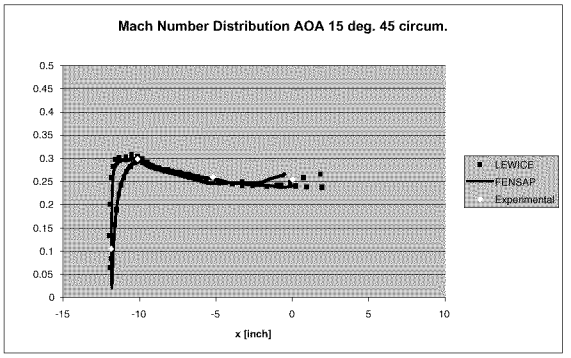

Figure 7: Mach number comparison for 15 deg. incidence and 45 deg. circumferential position

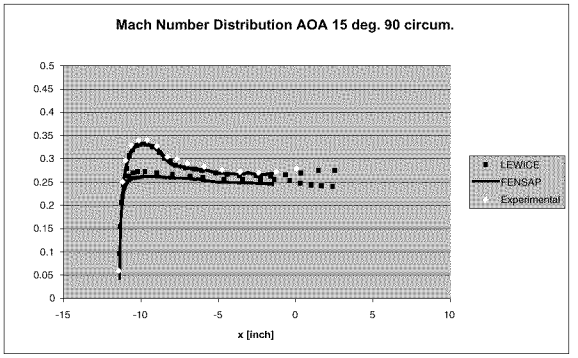

Figure 8: Mach number comparison for 15 deg. incidence and 90 deg. circumferential position

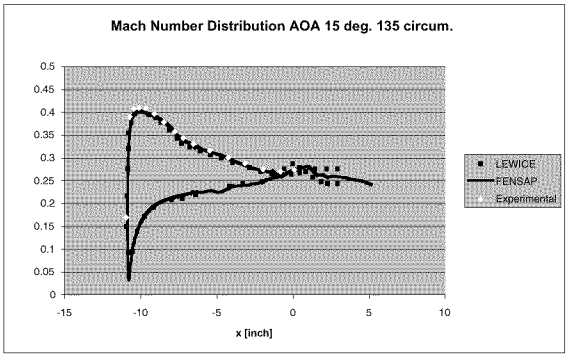

Figure 9: Mach number comparison for 15 deg. incidence and 135 deg. circumferential position

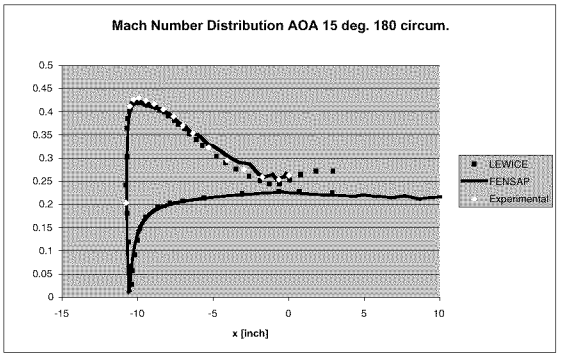

Figure 10: Mach number comparison for 15 deg. incidence and 180 deg. circumferential position

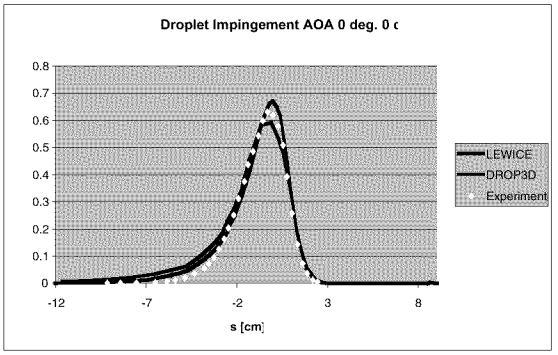

Figure 11: Local catch efficiency comparison for zero incidence and 0 deg. circumferential position

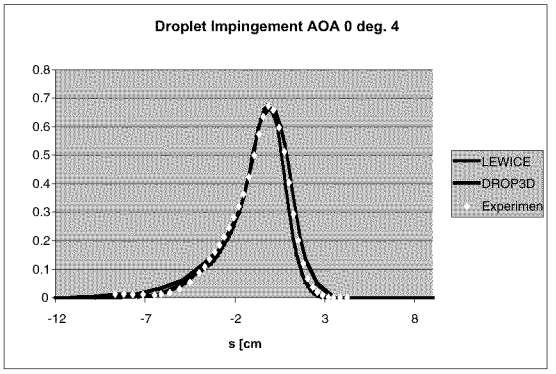

Figure 12: Local catch efficiency comparison for zero incidence and 45 deg. circumferential position

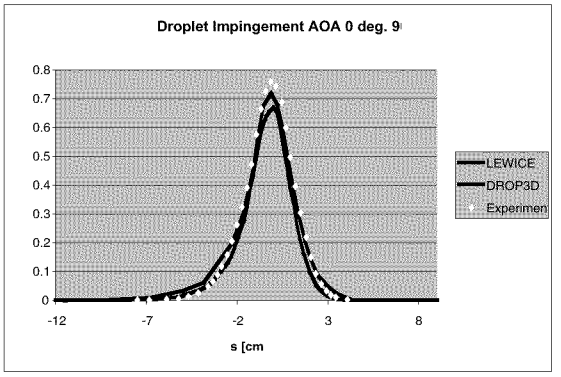

Figure 13: Local catch efficiency comparison for zero incidence and 90 deg. circumferential position

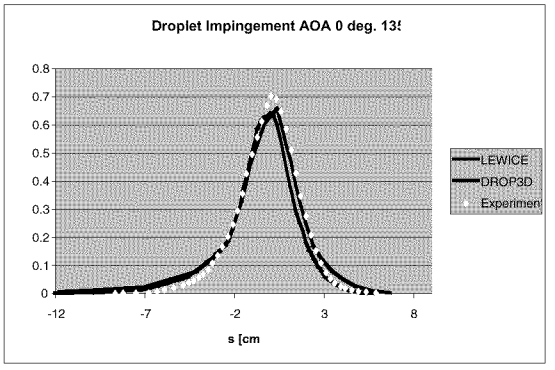

Figure 14: Local catch efficiency comparison for zero incidence and 135 deg. circumferential position

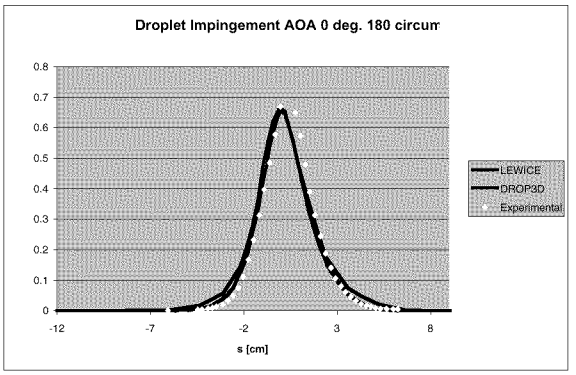

Figure 15: Local catch efficiency comparison for zero incidence and 180 deg. circumferential position

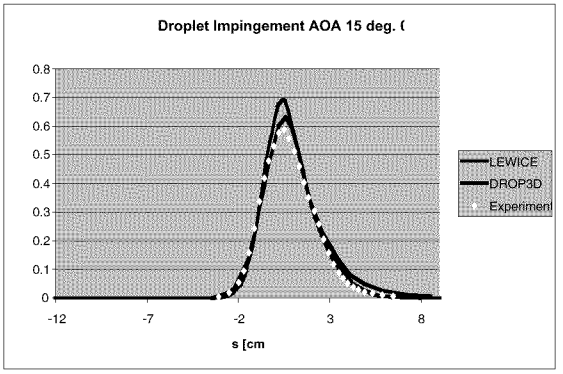

Figure 16: Local catch efficiency comparison for 15 deg. incidence and 0 deg. circumferential position

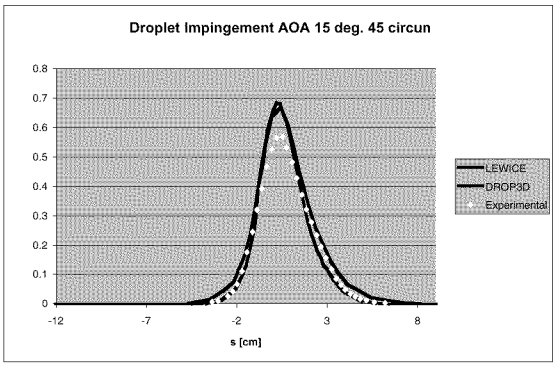

Figure 17: Local catch efficiency comparison for 15 deg. incidence and 45 deg. circumferential position

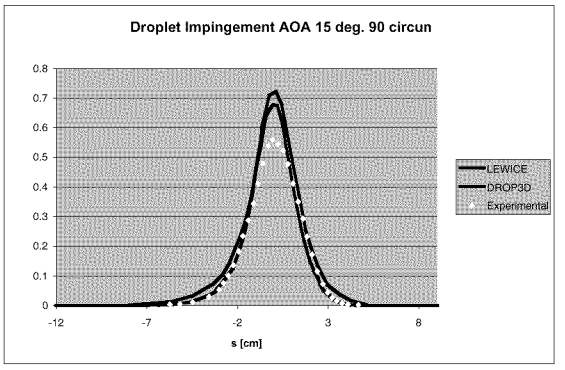

Figure 18: Local catch efficiency comparison for 15 deg. incidence and 90 deg. circumferential position

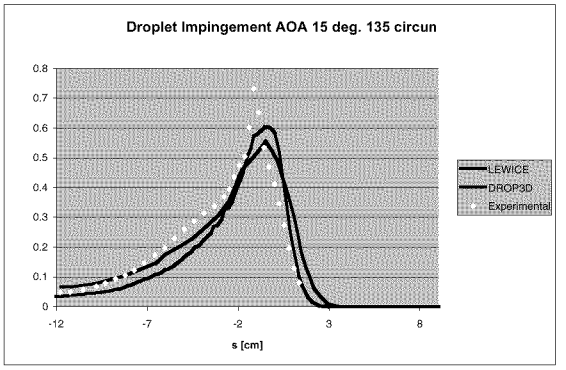

Figure 19: Local catch efficiency comparison for 15 deg. incidence and 135 deg. circumferential position

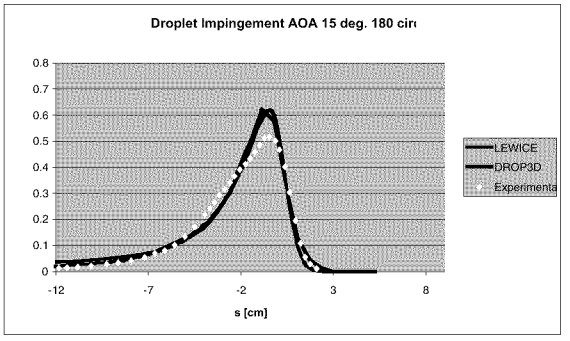

Figure 20: Local catch efficiency comparison for 15 deg. incidence and 180 deg. circumferential position

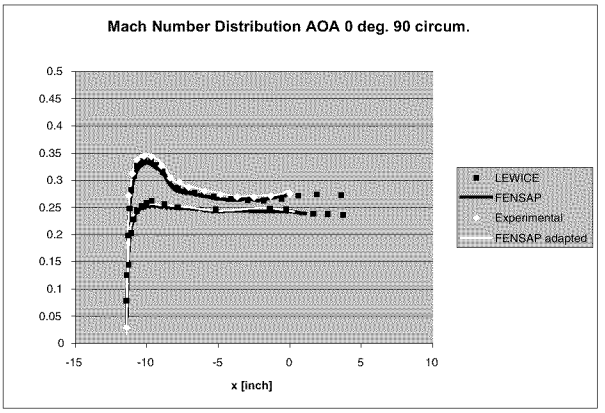

Figure 21: Mach number comparison for 15 deg. incidence and 90 deg. circumferential position, with mesh adaptation

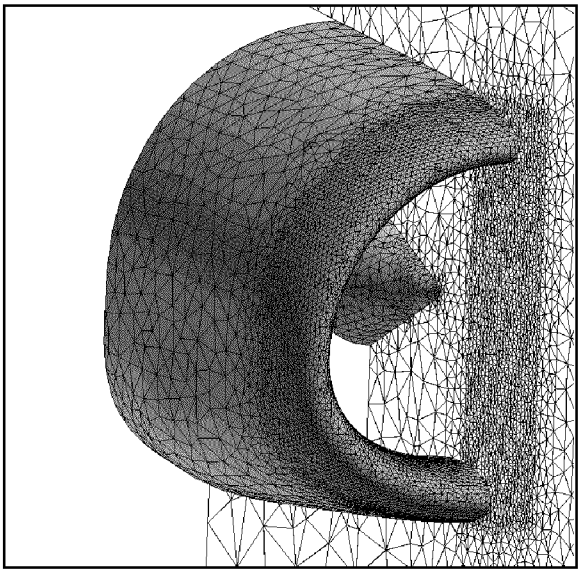

Figure 22: Tetrahedral unadapted mesh on nacelle and symmetry plane

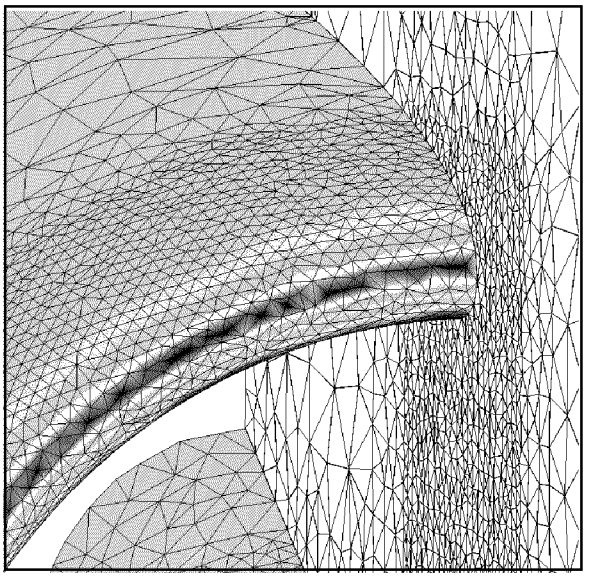

Figure 23: Unadapted mesh and Mach number distribution on nacelle and symmetry plane

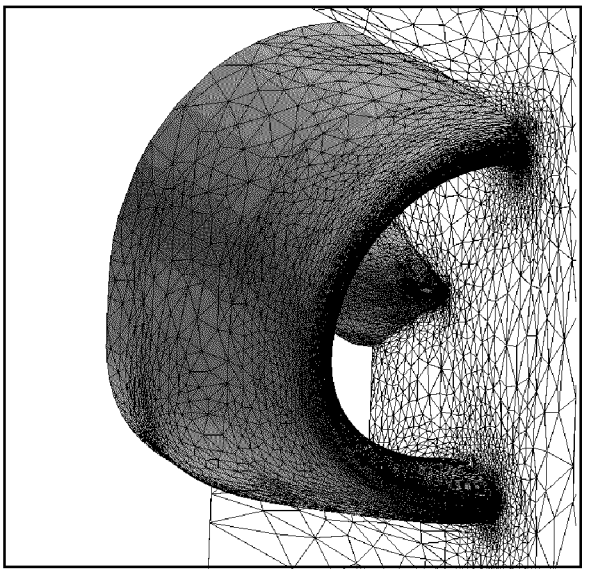

Figure 24: Tetrahedral adapted mesh on nacelle and symmetry plane

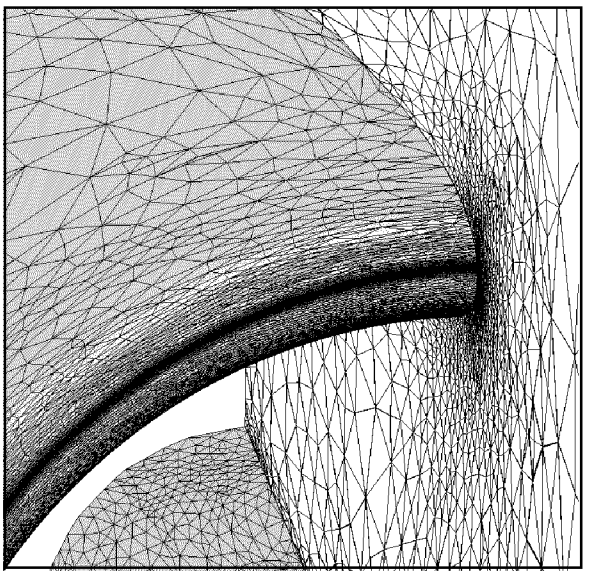

Figure 25: Adapted mesh and Mach number distribution on nacelle and symmetry plane

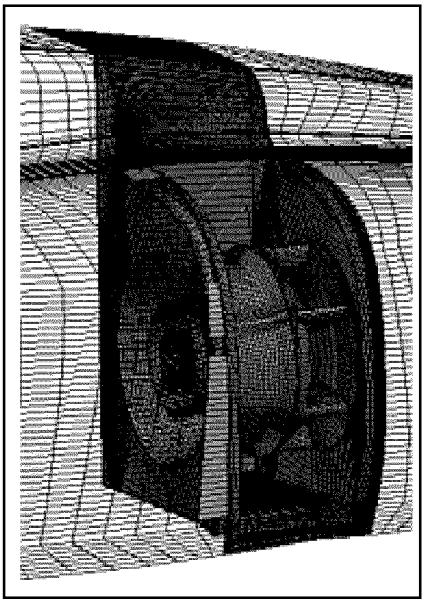

Figure 26: Hexahedral mesh on side-facing helicopter inlet

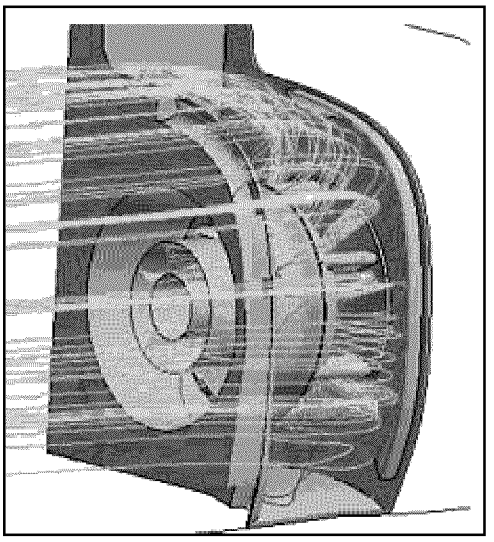

Figure 27: Streamlines on side-facing helicopter inlet

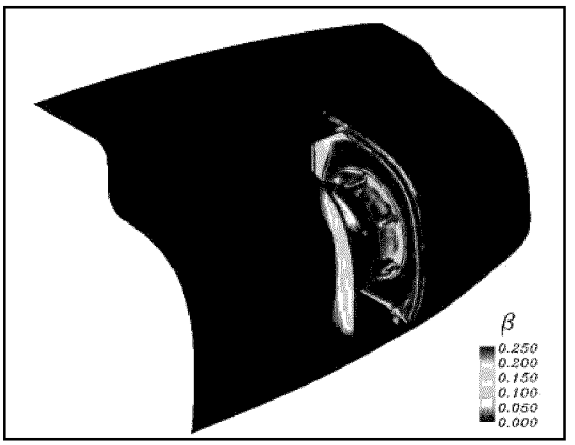

Figure 28: Catch efficiency distribution in helicopter engine compartment

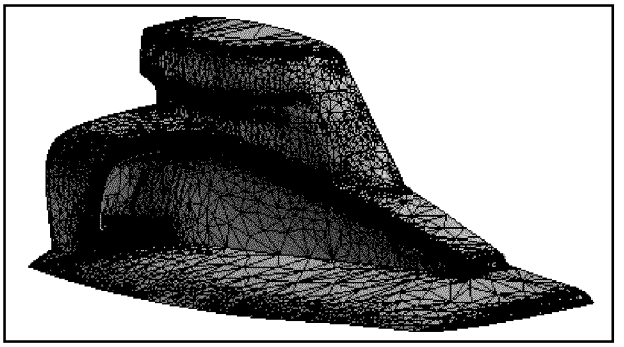

Figure 29: Tetrahedral adapted mesh on forward-facing helicopter inlet and upper cowl

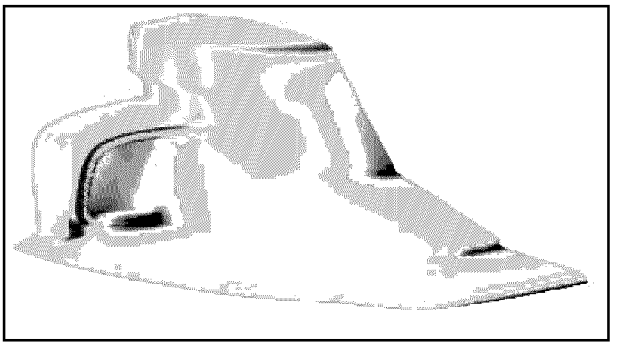

Figure 30: Mach number distribution on helicopter forward-facing inlet and upper cowl

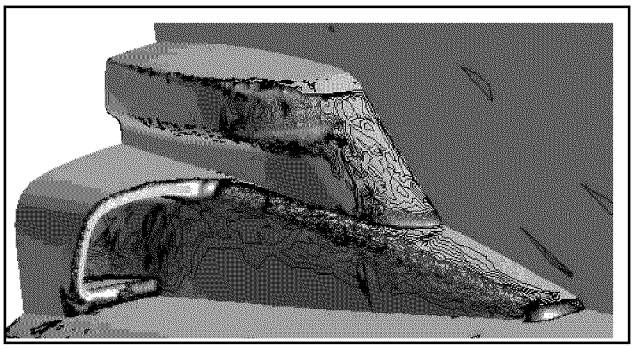

Figure 31: Catch efficiency distribution on helicopter forward-facing inlet and upper cowl

Figure 32: A 3D state-of-the-art Integrated System for Aerodynamics, In-Flight Icing Simulation and Certification

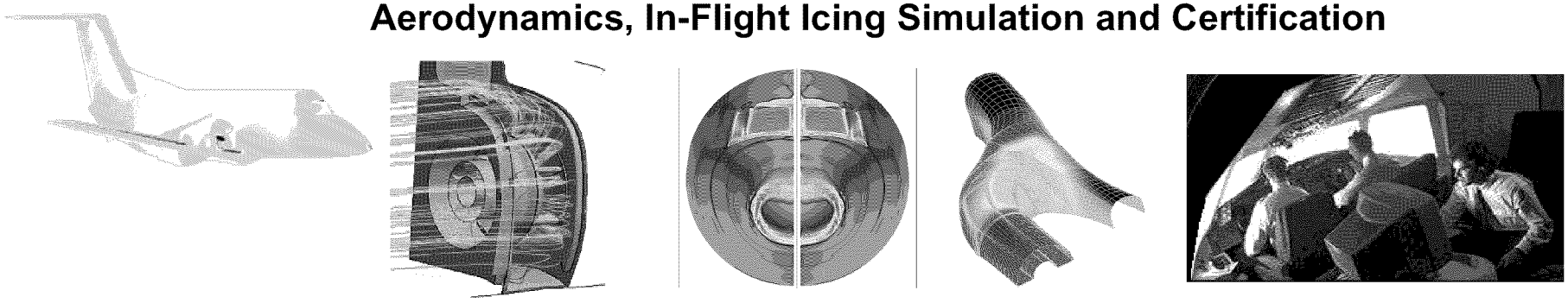

Turboprops Helicopters Turbojets Intakes Simulators

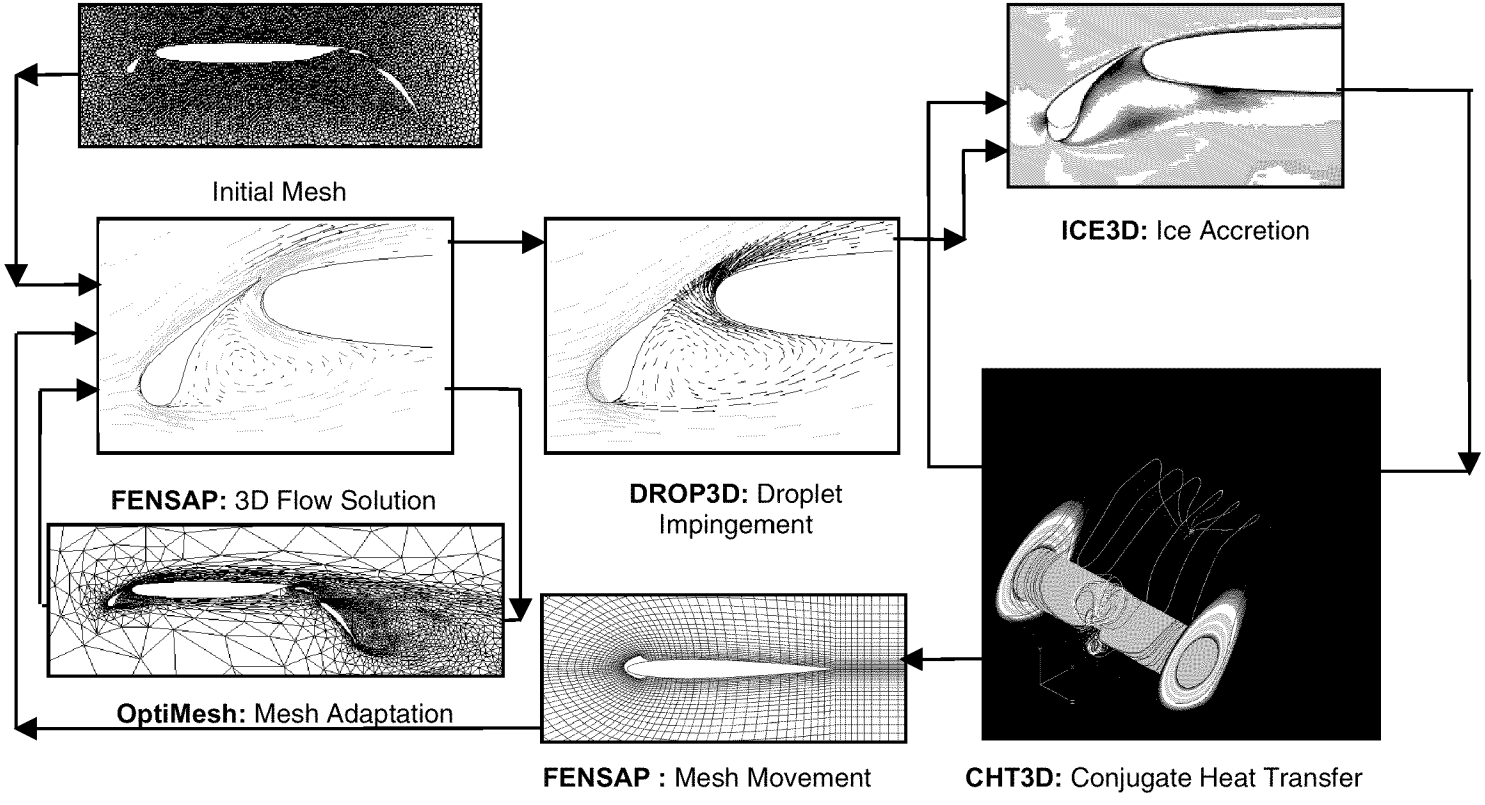

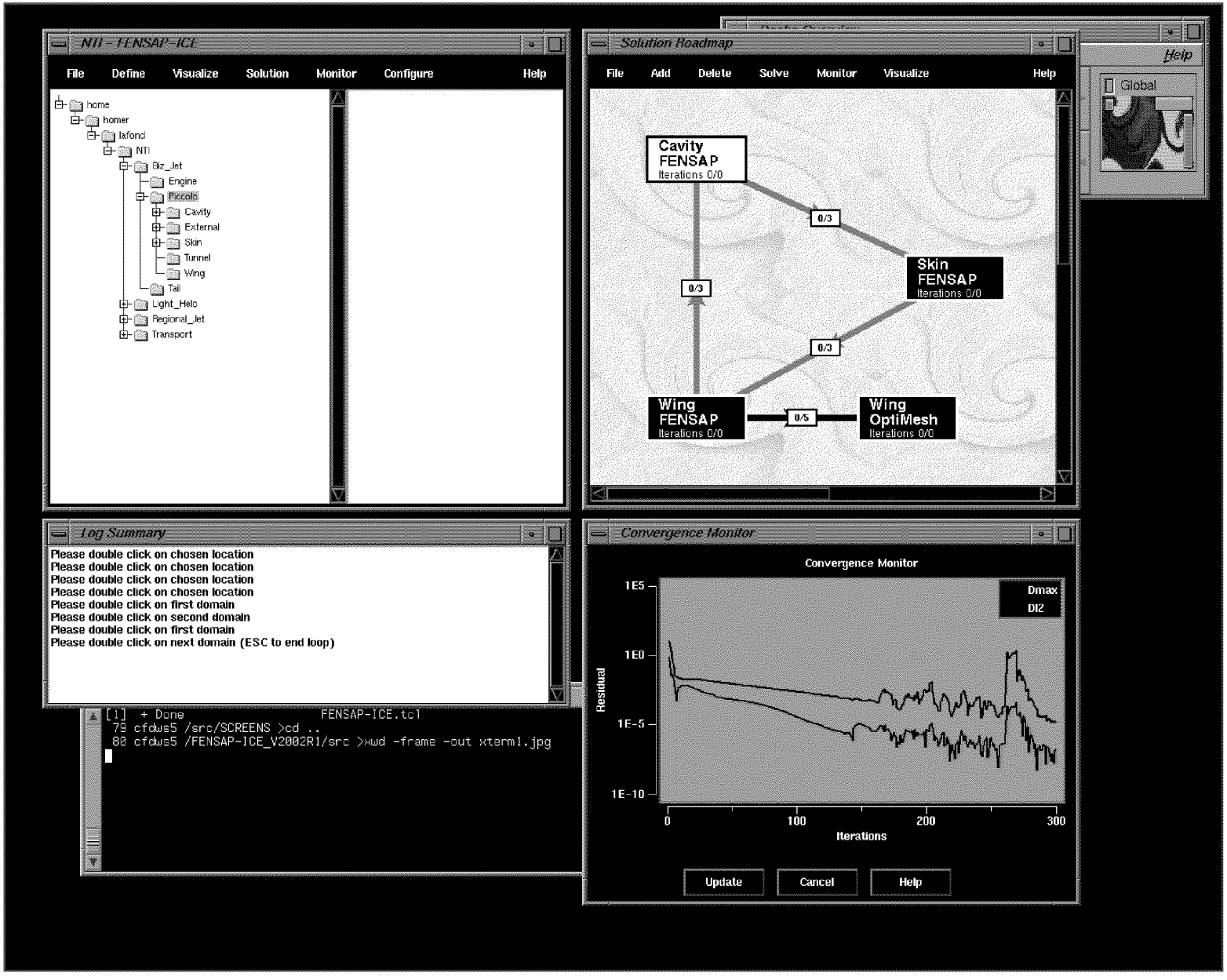
NTI - FENSAP-ICE
File
Define
Visualize
Solution
Monitor
Configure
Help
home
homer
lafond
NTI
Biz_Jet
Engine
Piccolo
Cavity
External
Skin
Tunnel
Wing
Tail
Light_Helo
Regional_Jet
Transport
Solution Roadmap
File
Add
Delete
Solve
Monitor
Visualize
Help
Cavity
FENSAP
Iterations 0/0
0/3
Skin
FENSAP
Iterations 0/0
0/3
0/3
Wing
FENSAP
Iterations 0/0
0/5
Wing
OptiMesh
Iterations 0/0
Help
Global
Log Summary
Please double click on chosen location
Please double click on chosen location
Please double click on chosen location
Please double click on chosen location
Please double click on first domain
Please double click on second domain
Please double click on first domain
Please double click on next domain (ESC to end loop)
[1] + Done FENSAP-ICE.tcl
79 cfdws5 /src/SCREENS >cd ..
80 cfdws5 /FENSAP-ICE_V2002R1/src >xwd -frame -out xterm1.jpg
Convergence Monitor
Convergence Monitor
Dmax
DI2
1E5
1E0
1E-5
1E-10
Residual
0
100
200
300
Iterations
Update
Cancel
Help